Additional pga ground-shaking and surface deformation hazard studies for the Wrights Road storage ponds

G.H. McVerry R.J. Van Dissen C.J. Van Houtte
I. Hamling C. Williams

GNS Science Consultancy Report 2015/221
December 2015

DISCLAIMER

Use of Data:

Date that GNS Science can use associated data: December 2015

BIBLIOGRAPHIC REFERENCE

McVerry, G.H.; Van Dissen, R.J.; Van Houtte, C.J.; Hamling, I.; Williams, C. 2015. Additional pga ground-shaking and surface deformation hazard studies for the Wrights Road storage ponds, *GNS Science Consultancy Report* 2015/221. 34 p.

CONTENTS

FIGURES

TABLES

EXECUTIVE SUMMARY

Additional studies of pga ground-shaking hazard and surface deformations have been performed for the Wrights Road Storage Ponds to assist Waimakariri Irrigation Limited (WIL) in defending the appeal against its grant of a resource consent for the project. This report presents the technical detail related to the supplementary evidence to be presented by Dr Graeme McVerry and Mr Russ Van Dissen of GNS Science at the reconvened appeal hearing in the Environment Court early in the new year of 2016.

The additional work included: the impact on probabilistic hazard results of entertaining shorter recurrence intervals for the Hororata Fault and four other fault sources in the region; the potential impact of “hanging wall” effects on the deterministic scenario hazard result for the Hororata Fault; the potential for ground deformation at the site resulting from rupture of the Hororata Fault; and comment on horizontal accelerations adjacent to intersections of reverse/strike-slip faults, vertical motions, ground deformations and subsoil class.

The introduction of hanging-wall factors for motions produced by the Hororata Fault resulted in an increase of 50% in scenario rock pga motions, which translated to an increase of nearly 40% over the original scenario results for the soil motions at the Wrights Pond site for the worst case (from 0.65g to 0.91g). However, the original 10,000-year design pga motions (1.11g) are over 20% stronger than even the 40%-enhanced scenario motions (0.91g).

The large changes in the scenario estimates do not flow through into the probabilistic hazard estimates of the 10,000-year pgas, on which the Safety Evaluation Earthquake (SEE) motions used for design are based. The new calculations demonstrate that the recommended 10,000-year pgas are insensitive to large changes in fault-rupture recurrence intervals for five of the near-by faults affecting the site, reductions in the source-to-site distance and enhancement of pgas by hanging-wall (or other) effects. The greatest increase found from the sensitivity studies was less than 5%, from 1.11g to 1.16g for the unweighted 10,000-year pga, for a case combining the simultaneous application of these multiple conservative assumptions.

This insensitivity arises because of the domination of the hazard estimates by the distributed-seismicity component of the earthquake model, which has very high earthquake rates to represent the on-going, although gradually decreasing, Canterbury earthquake sequence.

Consequently, it is concluded that the design SEE pga of 1.11g based on the 1/10,000 AEP value derived from a probabilistic seismic hazard analysis remains appropriate.

Additional ground deformation modelling and topographic analyses were undertaken to address issues raised at the Seismic Experts – Expert Witness Conference (16 September, 2015).

Approximately 50 different scenario Hororata Fault ruptures were evaluated using a combination of elastic dislocation and finite element modelling techniques, in order to characterise the amount of ground surface deformation that could be expected at the WIL Storage Pond site resulting from those scenario Hororata Fault ruptures. Rupture scenarios sampled reasonable ranges in fault dip (55°–75° NW), top depth of rupture (0.5–1.5 km), distribution of slip on the fault plane (uniform and variable), source to site distance (~4–8 km), and material properties of geological units (uniform and layered). In all cases, our modelled results predict tilts of less than 20 cm/km at the WIL Storage Pond site, and strains (both horizontal and vertical) of less than 50 µstrain (5.0×10^{-5} strain). Tilts and strains of these magnitudes are well within the tolerable limits of WIL Storage Pond structure, as supplied to GNS Science by Dam Watch Engineering.

Additional analysis of topography through the WIL Storage Pond site and to the east further affirms conclusions previously expressed in evidence presented by GNS Science. There is no direct evidence that surface fault rupture deformation expressed as either discrete faulting (i.e., a fault scarp), km-scale wavelength folding (anticlinal or synclinal), or differential tilting has impacted the location of the WIL Storage Pond site within the last approximately 18,000 years.

1.0 INTRODUCTION

This report presents the technical detail related to the supplementary evidence to be presented by Dr Graeme McVerry and Mr Russ Van Dissen of GNS Science at the reconvened appeal hearing in the Environment Court early in the 2016 new year relating to the granting of a resource consent to Waimakariri Irrigation Limited (WIL) for the construction and use of the Wrights Road Storage Ponds. The purpose of the report is to develop and present additional evidence in response to the appellants, and to provide the additional seismic hazard information required because of the replacement of the 2000 version of the *New Zealand Dam Safety Guidelines* by the much more detailed 2015 version (NZSOLD 2000, 2015). The intention is to address the issues raised in the statement of 25 September 2015 arising from the conference of seismic experts ordered by the Environment Court.

The detailed scope is presented in the Technical Brief.

2.0 TECHNICAL BRIEF

GNS Science proposes the following additional studies for the Wrights Road Ponds to address issues that have arisen during the Resource Consent appeal hearing and to satisfy the requirements of the 2015 NZSOLD *New Zealand Dam Safety Guidelines* that have been published since GNS Science carried out its hazard studies and prepared its evidence for the appeal hearing:

1. **Impact on probabilistic hazard results of entertaining a shorter recurrence interval for the Hororata Fault.**

   This point repeatedly comes up in questions raised by expert witness J. Campbell. GNS consider that it would be a valuable exercise to run the previously used hazard model, with modified recurrence intervals for rupture of the Hororata Fault. We anticipate this change will have little impact on the resulting hazard estimates, but we also consider it important to demonstrate that this is the case.

2. **The potential impact of “hanging wall” effects on the deterministic hazard result of the Hororara Fault, and the appropriateness of even considering that these effects may be suitable to apply to the WIL site.**

   Since presentation of GNS’s original hazard results for the WIL site in 2012, a number of “hanging wall” relationships have been published that relate to this question – most of these relationships were published in 2014. In addition, GNS has completed work at another dam site (unfortunately, confidential) that would indicate that, at least in that case, geological observations indicate that “hanging wall” effects do not appear to be as strong as indicated by the model near the end of the reverse fault in question. These observations are relevant to the WIL site, which is very close to the end of a reverse fault (the Hororata Fault). GNS Science will also provide an approximate indication of the effect of hanging wall factors on the probabilistic estimates for the pga estimates.

3. **Potential for ground deformation at the site resulting from rupture of the Hororata Fault.**

   GNS will undertake a more thorough assessment of this issue (compared to what Russ Van Dissen presented in his most recent round to evidence) to demonstrate that the numerous suppositions and plausibilities that J Campbell raised in new material that she presented at the Expert Witness conference are, in all likelihood, un-founded. Regardless of whether the objectors present this new material as evidence, GNS considers it will still likely comprise a line of questioning during cross examination.

4. **Reformat and supplement evidence relating to points covered in the Seismic Expert Witnesses Conference, including:**

   i. Horizontal accelerations adjacent to intersections of reverse/strike-slip faults
   ii. Vertical motions
   iii. Ground deformations
   iv. Subsoil Class

The material relating to items 1–3 will be presented in a GNS Science Consultancy report. Any new information from these studies that modifies or supplements previous evidence produced by GNS Science will also be formulated as evidence to be presented at the reconvened appeal hearing, together with additional evidence relating to item 4.

3.0 SEISMIC GROUND-SHAKING HAZARD

The first part of this report addresses issues related to the seismic ground-shaking hazard at the site of the proposed WIL storage ponds at Wrights Road identified as remaining points of contention in the Agreed Statement of 25 September 2015 arising out of the Expert Witness Conference of Seismic Experts held in Court Room 7 of the District Court in Christchurch on 16 September 2015.It also provides a broader range of sensitivity analyses of the recommended Safety Evaluation Earthquake (SEE) ground motions, consistent with the increased requirements for consideration of uncertainties in the New Zealand Dam Safety Guidelines (NZSOLD, 2015) compared with the requirements of the 2000 Guidelines that were current when the seismic hazard analyses for the Wrights Road Ponds were performed in 2012. The SEE motions were referred to as Maximum Design Earthquake (MDE) motions in the 2000 Guidelines.

3.1 EARTHQUAKE GROUND-SHAKING HAZARD ISSUES ADDRESSED IN THIS REPORT

The ground-shaking hazard issues addressed in this report relate primarily to the sensitivity of both probabilistic and deterministic (“scenario”) ground-shaking estimates to the recurrence intervals of several of the local faults, to the modelled location of the Hororata and Springbank Fault with respect to the ponds, and the effects of including hanging-wall factors for the Hororata Fault. The new material supplements the evidence previously submitted to the appeal hearing by Dr Graeme McVerry, namely his first statement of evidence dated 18 May 2015 and his first rebuttal evidence dated 24 July 2015. Specific issues addressed are:

1. A statement of probabilistic specification of the Safety Evaluation Earthquake (SEE) motions as given by the 2015 NZSOLD Large Dam Guidelines and the alternative deterministic (scenario) specification;
2. Modification of the location of the top of the modelled rupture surface and the dip of the Hororata Fault, based on the results of surface deformation studies discussed later in this report (Section 4) that will form the basis for supplementary evidence to be presented to the reconvened hearing by Mr Russ Van Dissen;
3. The sensitivity of the hazard estimates to the range of rupture-recurrence intervals for the Hororata, Springbank, Ashley and Porters Pass Faults identified in the June 2015 evidence of Mrs Jocelyn Campbell that was submitted to the Appeal Hearing;
4. The estimation of the range of hanging-wall factors for Hororata Fault pgas at the Wrights Road Ponds;
5. The application of these hanging-wall factors to the Hororata Fault for both the scenario and probabilistic ground-shaking hazard estimates;
6. Demonstration of the conservatism of the 10,000-year peak ground acceleration hazard estimates recommended as the SEE motions, by their insensitivity to the combined effect of all modifications listed under items 2 to 4.

The sensitivity studies were carried through fully only for the unweighted horizontal peak ground accelerations (pgas), as Dam Watch Engineering Ltd advised GNS Science that magnitude-weighted pgas, response spectra, vertical pgas and acceleration histories were not required for the design. Subsequently, Dam Watch informed GNS Science that spectral accelerations at periods of 0.10s and 0.19s were also used. Given the shortness of these spectral periods, it is likely that they will show similar (lack of) sensitivity to the factors considered in the sensitivity studies for pga.

3.2 SAFETY EVALUATION EARTHQUAKE MOTIONS

There are clear guidelines as to the required design levels for dams and similar structures in New Zealand. The *New Zealand Dam Safety Guidelines* (NZSOLD, 2015) allow the use of either scenario motions at the 84th-percentile level or probabilistically-derived motions with an annual exceedance probability (AEP) of 1/10,000 as alternative specifications of the Safety Evaluation Earthquake (SEE) motions for Potential Impact Category (PIC) 3 dams, the highest PIC level, which governs the Wrights Road storage ponds. The scenario motions need not exceed the 1/10,000 AEP motions. It is not required to consider worst-case or extreme possibilities without regard to the probabilities of those cases occurring.

In the hazard studies performed for the Wrights Road storage ponds in 2012, the 1/10,000 AEP motions encompassed those estimated for all reasonable scenarios, including those for shorter distances or larger magnitudes than estimated for any of the local faults. It is shown later in this report that the recent sensitivity studies demonstrate that the original 1/10,000 AEP motions continue to exceed scenario motions even with large changes in the fault parameters and considerably increased scenario ground-motion estimates.

3.3 UNCERTAINTY IN FAULT CHARACTERISATION

Much of the evidence submitted to the Appeal Hearing by Ms Jocelyn Campbell on behalf of the appellants was related to a discussion of the degree of uncertainty in the characterisation of faults in the region around the Wrights Road Storage Ponds, especially the Hororata Fault Zone. Her evidence makes no attempt to quantify the probabilities of various fault-rupture scenarios occurring. Neither does it quantify the effect of these uncertainties on the estimated ground-shaking hazard or ground deformations that form the basis for the design. In the current report, it is demonstrated that many of these uncertainties have little effect on the earthquake ground-shaking hazard estimates on which the recommended design motions were based.

The lack of sensitivity to these uncertainties is mainly because the fault sources to which the uncertainties relate make little contribution to the overall hazard estimates.

As stated in paragraph 21 of the first statement of evidence by Dr McVerry, the seismicity model used by GNS Science for the hazard estimates for the site of the proposed Wrights Road storage ponds consists of two components: 1) a fault source component, and 2) a grid of distributed seismicity that accounts for earthquakes not assigned to specific faults.

The gridded seismicity is a smoothed representation of the historical seismicity, including the current Canterbury earthquake sequence up to 15 January 2012. The gridded seismicity includes magnitudes up to 7.2, as large as that assigned to the Hororata Fault and larger than the September 2010 Darfield earthquake.

The current and on-going, although gradually diminishing, seismicity rates associated with the current earthquake sequence far exceed those in Canterbury prior to the September 2010 Darfield earthquake (Gerstenberger et al. 2014). Consequently, the gridded seismicity contributes virtually all of the estimated ground-shaking hazard at the Wrights Road pond sites (paragraph 44 of Dr McVerry's statement of evidence), far exceeding that of the faults on which Ms Campbell focussed much of her evidence. The contribution of the on-going earthquake sequence is largely overlooked in Ms Campbell's evidence. The relative contributions of the modelled fault sources and the distributed seismicity grid are quantified later in this report (Section 3.7 and Table 3.2).

3.4 MODELLED GEOMETRY OF THE POND SITES AND CLOSEST FAULTS

For the hazard results presented in Dr McVerry's evidence dated 18 May 2015 and 24 July 2015, the representations of the faults in the vicinity of the Wrights Road Ponds were taken as given in GNS Science's National Seismic Hazard Model (NSHM), as published in Stirling et al. (2012).The NSHM fault representations were developed on a country-wide basis.

Two changes have been made to the modelled geometry of the Hororata Fault in terms of its location relative to its associated anticline and Wrights Road Ponds, in light of more detailed knowledge gained from studies performed for the project. The Hororata Fault and its associated anticline and the current modelling of their relationship are discussed in Sections 4.2 and 4.3 and Tables 4.2 and 4.3.

Firstly, the modelled location and dip of the fault have been modified to be consistent with the crest of its associated anticline, as determined from the recent deformation modelling carried out by GNS Science as part of the current study. The deformation modelling was required to determine the location of the fault because it has no surface trace at its closest approach to the pond sites to constrain its dip and location by direct observations in the vicinity of the ponds.

Secondly, the location chosen for the hazard calculations has been modified to that closest to the new modelled location of the Hororata Fault (south-east corner of the footprint of the ponds).

These changes have reduced the shortest modelled fault-to-site distances from 5.4 km to 4.8 km for the Hororata Fault.

The modelled location of the Springbank Fault is unchanged from the National Seismic Hazard Model (Stirling et al. 2012), but the revised location used for the site reduces its shortest distance from the site from 3.0 km to 1.1 km.

The modelled geometry and fault locations for both the Hororata and Springbank Faults produce pga estimates that are expected to be conservative (i.e., on the high side).

The modelled location of the Springbank Fault extends considerably closer to the ponds than is necessary in terms of its surface expression. The extension of the Springbank Fault in the NSHM beyond its surface expression is to satisfy "scaling relations" between fault displacement, magnitude, length and width (i.e., to produce the length that is consistent with the average associated with its estimated magnitude). Considerably shorter lengths than the average, consistent with the surface expression, could be justified because of the large degree of scatter in magnitude versus rupture length correlations.

In the previous studies for the Wrights Road Ponds and the new sensitivity studies, the representation of the Springbank Fault as given in the pre-existing NSHM was retained on the grounds of conservatism, rather than reducing its length to be more consistent with its surface expression.

The conservatism of the representation of some of the faults in the region was mentioned in Dr McVerry's evidence of 18 May 2015 (paragraph 23), including direct reference to the Springbank Fault (paragraph 53), and again in his statement of evidence-in-reply of 24 July 2015 (paragraph 9).

Consequently, the short distance of the modelled Springbank Fault from the pond site is an artefact resulting from the fault being modelled as extending well beyond its surface manifestation to the vicinity of the ponds. In reality, it is likely to lie at a greater distance from the pond site.

Accordingly, the Hororata Fault rather than the Springbank Fault is the fault that has been considered for both ground deformation and hanging wall effects.

3.5 RECURRENCE INTERVALS OF FAULT RUPTURE

Tables 1 to 4 of Ms Campbell's evidence submitted for the appeal hearing provided listings of the wide ranges of recurrence intervals (RIs) of rupture that have been published for the Hororata, Ashley, Springbank and Porters Pass faults.

For the purpose of the sensitivity studies reported here, the RIs for the Hororata, Ashley, Springbank and Porters-Grey-S (shorter) faults have been reduced simultaneously to the shortest values given in Tables 1 to 4 of Ms Campbell's evidence. The RI for the Porters-Grey-L (longer) Fault has also been reduced considerably from the previous GNS model. This does not indicate acceptance by GNS Science of the reduced recurrence intervals, but is to provide a demonstration of the lack of sensitivity of the probabilistic hazard estimates over very wide ranges of the recurrence intervals. The RI values used in the previous GNS Science hazard studies and those used for these sensitivity studies are listed in Table 3.1.

The effects of these large changes in the RIs on the results of the hazard analysis are presented after discussion of other changes to the inputs to the analyses.

Table 3.1 Recurrence intervals (RIs) used in the previous GNS hazard estimates and for the current sensitivity studies.

Fault	RIs (years) used in previous GNS Science study	RIs (years) used in current sensitivity studies
Hororata	17,000	4800
Ashley	4900	2000
Springbank	12,000	7200
Porters-Grey-S (shorter)	1900	700
Porters-Grey-L (longer)	8400	2000

3.6 HANGING-WALL FACTORS

Hanging-wall effects were not included previously in either the probabilistic or scenario hazard analyses. This was partly because their estimates are highly-dependent on the geometry of the fault-rupture surface with respect to the location of the site, which, as Ms Campbell has pointed out, is uncertain. Also, adequate models for hanging-wall effects were lacking, but became available in 2014.

Hanging-wall effects refer to the observation that ground motions on the block lying above the fault plane (i.e., the hanging wall) of a dipping fault plane tend to be larger than those on the footwall. The hanging wall and foot wall of a dipping fault are depicted in Figure 3.1. Hanging wall sites are located closer to a larger part of the source plane than those on the foot-wall, and hence are exposed to higher seismic energy.

Hanging-wall factors may affect the storage pond sites for motions caused by the Hororata Fault. In terms of the NSHM fault representations, they may possibly affect the motions at the site from the Springbank Fault, but in reality this fault is likely to be sufficiently distant from the pond sites that any hanging-wall effects it produces there are likely to be insignificant.

The hanging-wall factors for motions caused by the Hororata Fault were first estimated at the site of the ponds, as described in the remainder of this section. The estimated hanging-wall factors for motions produced by the Hororata Fault were then introduced into the probabilistic estimates of the 1/10,000 AEP pgas, as discussed in Section 3.7.

A total of 18 combinations of locations, orientations and slip distributions for the Hororata Fault were considered. Each of these gave surface deformations consistent with those observed, particularly in regard to reproducing the location of the crest of the anticline associated with this fault. The work related to matching the surface deformations is reported in Sections 4.2 to 4.4, and will be presented in the supplementary evidence of Mr Van Dissen.

The enhancements of the pgas at the pond site were then calculated for each of the 18 models of the Hororata Fault using three recent models for estimating hanging-wall factors.

The three hanging-wall models considered for this project were: 1) the Abrahamson, Silva and Kamai (2014; ASK14) model, 2) the Campbell and Bozorgnia (2014; CB14) model, and 3) the Chiou and Youngs (2014; CY14) model. These three models are widely considered the best models of the hanging-wall effect currently available. Given that there is a global paucity of recorded ground-motion data for sites located on a fault hanging wall, these three models are strongly based on the simulated dataset of Donahue and Abrahamson (2014).

The 18 scenarios considered were all possible combinations of:

1. Three alternative interpretations of the Hororata Fault dip, 55, 65 and 75 degrees;
2. Three different depths to the top of the rupture plane, 0.5, 1.0 and 1.5 km; and,
3. Two different assumptions on the slip distribution of the fault rupture, a constant slip model of 3 m, and a model with more slip concentrated towards the bottom of the fault (average slip of 3 m, but the bottom third of the fault plane having 5 m of slip, the middle third of the fault plane having 3 m of slip, and the top third of the fault plane having 1 m of slip).

The reason for considering these 18 scenarios is that the hanging-wall effect is strongly spatially dependent, and these scenarios sample the possible range of hanging-wall amplifications given the range of key uncertainties regarding the location and orientation (dip) of the fault.

Figure 3.1 shows the behaviour of the three hanging wall models in a fault perpendicular direction over the Hororata Fault. The scenario pictured has a dip of 65 degrees and assumes constant slip on the fault. Three different values of the top depth are shown, to illustrate that the different assumptions result in different locations of the fault with respect to the anticline and site, each associated with different hanging wall factors. The amplifications shown are for rock site motions.

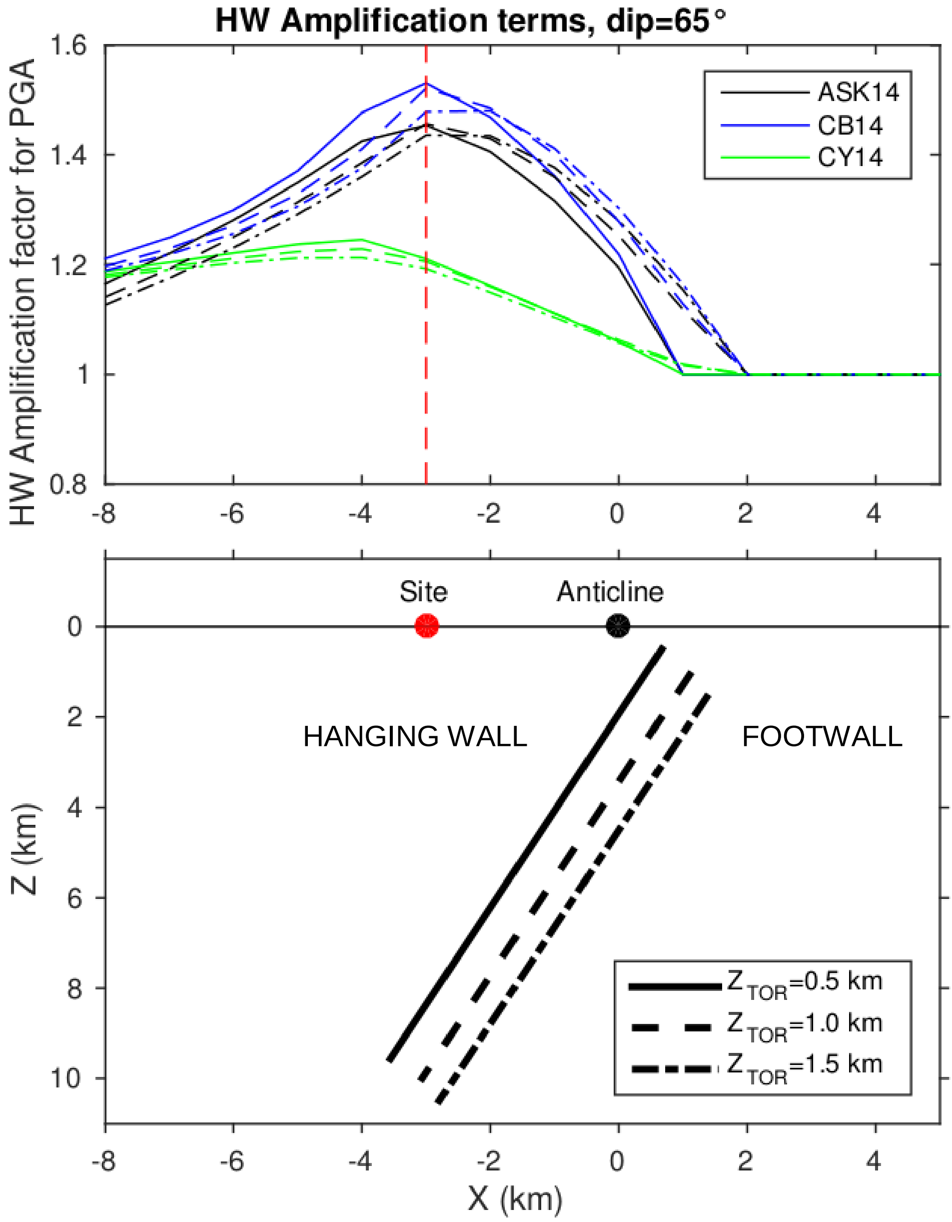

Figure 3.1 Amplification from hanging wall effects of rock motions at the site, as predicted by three hanging wall models for three of the 18 fault-geometry scenarios derived from deformation modelling. Bottom panel represents a fault-perpendicular slice through the Hororata Fault (X direction), showing the WIL site and anticline with respect to the three fault locations associated with a dip of 65° and a uniform distribution of slip on the fault plane. Z direction represents depth below ground surface. The subscript TOR stands for "top of rupture". Top panel represents the amplification of rock-site PGA for the three scenarios, as predicted by the three hanging wall models used in the analysis. Red dashed line represents the location of the WIL site.

Figure 3.2 shows the amplifications of pga from hanging-wall effects at the WIL site estimated for rock-site conditions for the 18 different scenarios and the three different hanging-wall models. It is clear from this figure that the hanging-wall amplification depends strongly on fault dip. The assumption of uniform slip or variable slip also affects the hanging-wall amplification, in the sense that the variable slip assumption shifts the fault location further from the WIL site and hence lowers the potential pga amplification.

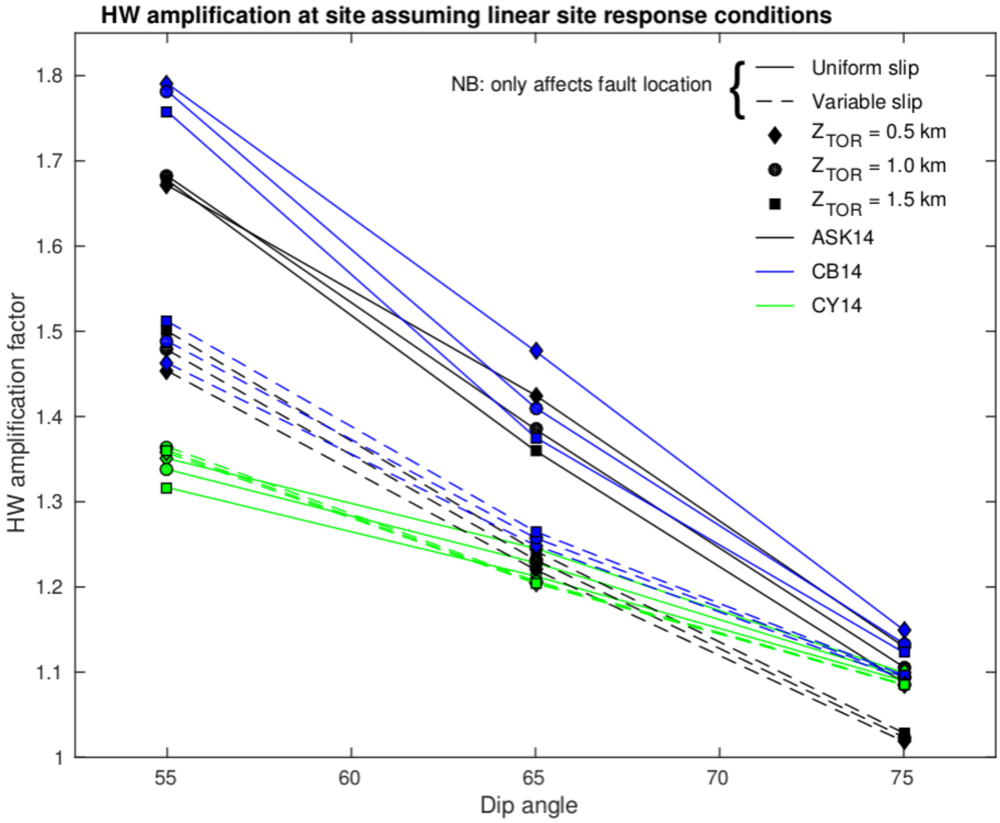

Figure 3.2 Range of hanging wall amplifications at the WIL site assuming rock site conditions (i.e., before reduction in pga motions from nonlinear soil response).

The results in Figure 3.1 and Figure 3.2 are for rock site conditions. In the probabilistic ground-shaking hazard analysis, the hanging-wall factors for rock conditions are combined with the nonlinear site response for the deep stiff gravel conditions at the site to obtain the corresponding modifications to the pgas for the ground conditions at the site. As the pga on rock increases, the relative amplification of soil motions is smaller due to nonlinear soil response. The stronger motions induce higher shear strains in the soil, which lower the effective shear modulus of the soil and increases its damping. This means that the hanging-wall amplification effects at the WIL site are likely to be smaller than those pictured in Figure 3.1 and Figure 3.2.

The hanging-wall factors for pga for rock site motions estimated from the fault scenario modelling were input to probabilistic hazard analyses for the site which incorporated the effect of nonlinear soil response. For the preferred dip angle of 65°, the hanging-wall factors at the WIL pond location for rock site conditions ranged from about 1.2 to about 1.5. The range results from the dependence of the hanging-wall factor on the selection of the ground motion prediction model, depth to the top of the rupture and distribution with depth of the slip over the fault-rupture surface.

Two sensitivity runs have been performed for the probabilistic model in which the calculated motions at the WIL pond site for Hororata Fault motions were enhanced by 1.2 and 1.5 for rock reference motions. The non-linear stress-strain characteristics used in the hazard calculations reduced these factors to 1.15 and 1.36, respectively, for soil conditions appropriate to the site.

3.7 MODIFIED UNWEIGHTED PGA HAZARD ESTIMATES

The pga sensitivity studies have been performed only for the McVerry stress-drop enhanced ground-motion prediction equation (GMPE), because the previous calculations showed that this model gave stronger pgas than the Bradley GMPE.

Table 3.2 shows the changes in the 50- and 84-percentile scenario estimates of pga motions for the Hororata Fault, for the shorter site-to-source distances, and rock pga hanging-wall factors of 1.2 and 1.5. These increase by nearly 40% from the original scenario results for the worst case (from 0.65g to 0.91g).

Results are also shown in Table 3.2 for the cumulative effects on the 10,000-year probabilistic estimates of pga from successively applying the effects of modified source-to-site distance, much reduced recurrence intervals of rupture for five of the faults affecting the site, and hanging-wall factors for Hororata Fault motions. In contrast to the large increase in the scenario pga estimates, there is less than 5% increase (from 1.11g to 1.16g) in the estimated 10,000-year pga when all these changes are applied simultaneously, a very conservative assumption.

The original 10,000-year design pga motions (1.11g) are over 20% stronger than even the 40%-enhanced scenario motions (0.91g).

The large difference between the percentage changes in the 10,000-year probabilistic estimates (current sensitivity study versus original GNS study) and the scenario Hororata Fault estimates (largely hanging-wall versus no hanging-wall effects) is because the probabilistic hazard estimates are dominated by contributions from the distributed seismicity model used to represent the on-going Canterbury earthquake sequence. This dominance (between 81% and 95% of the total contributions) is shown by the listing in Table 3.2 of the percentage contributions to the exceedance rates of the 10,000-year pgas from the Hororata Fault, all faults, and distributed seismicity.

For the original GNS model, the Hororata Fault produces less than 1% of the contribution. Even when all the conservative assumptions are lumped together, the contributions from the Hororata Fault grow to only about 13% of the exceedances of the 10,000-year pga.

The relative contributions of the Canterbury earthquake sequence model are 94% for the initial model, but are still 81% with the most conservative assumptions about the recurrence intervals and ground-motion modelling for the Hororata and other local faults.

Table 3.2 Scenario and probabilistic pga estimates and contributions to 10,000-year exceedance rates.

Model	Hororata Fault scenario PGA (g)		10,000-year probabilistic PGA (g)	Percentage contribution to exceedance rate of 10,000-yr PGA		
	50-percentile	84-percentile		Hororata Fault	All faults	Canterbury sequence distributed seismicity
1) Original	0.42	0.65	1.11	0.85	6	94
2) New geometry	0.43	0.67	1.13	0.9	5	95
3) Short RIs with (2)	0.43	0.67	1.14	3.0	9	91
4) 1.2 hanging-wall factor with (3)	0.49	0.77	1.15	6	12	88
5) 1.5 hanging-wall factor with (3)	0.58	0.91	1.16	13	19	81

3.8 OTHER FACTORS RELATED TO GROUND MOTIONS

3.8.1 Enhanced ground motions

Ms Campbell's evidence of June 2015 (paragraph 8) raises the possibility that "the characteristics of the underlying stratigraphy and structures in the vicinity of the WIL site… may modify the ground response to earthquakes emanating from these sources." Near-fault rupture directivity and polarisation, fault-fling, hanging-wall effects, anomalously large displacement: rupture length ratios, large vertical accelerations and trapping of energy by lower-velocity surface layers were among the issues raised.

The original estimates from the McVerry et al. GMPE were enhanced by stress-drop factors, in recognition that the ground motions recorded in Christchurch were stronger than predicted by the standard McVerry et al. (2006) ground-motion prediction equation (GMPE). Subsequently, hanging-wall factors were included as well.

The insensitivity of the results found for large increases in the hanging-wall factor show that any further enhancement to cover other issues, while increasing the scenario motions, would be unlikely to cause much increase in the probabilistic values.

3.8.2 Vertical accelerations

In Dr McVerry's previous evidence dated 24 July 2015, vertical pgas were also recommended, based on methods that take account of the statistical distribution of the ratio of near-field vertical to horizontal motions, rather than extreme values.

The vertical acceleration values have not been revisited, because of advice from Dam Watch Engineering Ltd that vertical pgas are not required for the design.

3.8.3 Site-class characterisation

Ms Campbell (paragraph 13) casts doubt on the assignment of NZS1170.5 Site Class D Deep or Soft Soil to the site. This is an issue that is not clear-cut, and Ms Campbell and GNS Science continue to disagree in their assessment. As discussed in paragraph 34 of Dr McVerry's previous evidence, the assessment of GNS Science geophysicist Dr Anna Kaiser, is that the site is probably Class D, but that can't be stated with absolute certainty.

3.9 SUMMARY OF RESULTS OF PGA SENSITIVITY STUDIES

The new calculations demonstrate that the recommended 10,000-year pgas are insensitive to large changes in fault-rupture recurrence intervals and enhancement of pgas by hanging-wall (or other) effects.

This insensitivity arises because of the domination of the hazard estimates by the distributed-seismicity component of the earthquake model, which has very high earthquake rates to represent the on-going, although gradually decreasing, Canterbury earthquake sequence.

The appellants have concentrated on uncertainties in the fault modelling and their associated levels of ground-shaking, without recognising the very high (but data-based) seismicity rates assigned to the on-going sequence that overwhelm the effects of the uncertainties in the fault modelling.

This approach of assessing the sensitivity to uncertainties in the hazard modelling contrasts with that of Ms Campbell, who in many cases presents worst-case or extreme possibilities, with no attempt to indicate the probabilities of these cases occurring.

The calculations confirm statements made in Dr McVerry's previous evidence that were based on his experience from performing many probabilistic seismic hazard estimates.

The calculations confirm that the hanging-wall effect has a large impact on the scenario pgas for the Hororata Fault, but only a minimal impact on the probabilistic pgas, because the bulk of the contributions to even the 1/10,000 Annual Exceedance Probability pga comes from sources other than the Hororata Fault.

The inclusion of hanging-wall factors narrows the gap between the probabilistic and scenario pga estimates, but the minor changes to the probabilistic estimates do not greatly affect the values selected for design.

The earthquake ground-shaking values recommended for the design are robust and conservative. As well as the sensitivity studies presented in the current supplementary report, the comments from Dr McVerry's previous evidence about the conservatism of the models and treatment of the results used in deriving the recommended design motions are reiterated, namely:

1. The results are based on earthquake recurrence models that take account of the currently enhanced seismicity rates in the Canterbury region from the on-going earthquake sequence, and allow for the possibility of stronger than usual motions through adding stress-drop enhancement factors to the McVerry et al. GMPE.
2. A conservative approach of equalling or exceeding the values calculated from the alternative Bradley (2010, 2013) and stress-drop enhanced McVerry ground-motion models for the required AEPs was adopted.
3. As well as satisfying the 1/10,000 AEP criterion, the horizontal design pgas also exceed the strongest 84-percentile scenario values for any of the modelled faults, including consideration of hanging-wall effects, where appropriate.
4. The scenarios considered previously went further, to show that the recommended SEE motions also exceed those estimated by alternatively shortening the distance to zero or increasing the magnitude for the largest magnitude local fault.

The greatest increase found from the sensitivity studies was less than 5%, from 1.11g to 1.16g for the unweighted 10,000-year pga, for a case combining the application of multiple conservative assumptions.

Consequently, it is concluded that the SEE design earthquake pga of 1.11g based on the 1/10,000 AEP value derived from a probabilistic seismic hazard analysis remains appropriate.

4.0 GROUND-SURFACE FAULT RUPTURE HAZARD AT THE WIL STORAGE POND SITE

4.1 MOTIVATION FOR ADDITIONAL GROUND DEFORMATION INVESTIGATIONS

In Mr Van Dissen's evidence of 18 May 2015, he presented detailed Digital Elevation Models (DEMs), and topographic profiles derived from high-resolution LiDAR data to assess whether or not the ground surface at the WIL Storage Pond site has been adversely impacted in the past by fault rupture deformation. (These DEMs and topographic profiles were presented as Figures 1–6 of his evidence).

From these topographic data, and the ≥~18,000 year estimate for the age of the fan surface on which the WIL Storage Pond is located, Mr Van Dissen concluded that, within the resolution of the detailed topographic data, there was no evidence that surface fault rupture deformation has impacted the location of the WIL Storage Pond site within the last approximately 18,000 years (paragraphs 27-29 & 32 of Mr Van Dissen's 18 May 2015 evidence).

In paragraph 46 of Ms Campbell's evidence (May 2015), she states:

> *"The evidence of Mr van Dissen that the LiDAR data adequately demonstrates the absence of any fault scarp across the footprint of the WIL pond and that the topography is that of channels on a fan surface spilling off and around Burnt Hill ia [is] not disputed."*

In addition, at the Seismic Experts – Expert Witness Conference (16 September 2015: point 6) it was agreed that:

> *"Surface rupture is unlikely through the site."*

However, Ms Campbell does question whether or not the site could have been subjected to tectonic tilt. And, related to this, it was agreed at the Seismic Experts – Expert Witness Conference (16 September 2015: point 7) that:

> *"Tilting and straining of the ground surface at the site is likely in the event of rupture of the Hororata Fault which is the CME [Controlling Maximum Earthquake] event in a deterministic sense."*

In Mr Van Dissen's July 2015 evidence (paragraphs 24-39), he presented additional Lidar-based topographic analysis and elastic dislocation modelling results of scenario Hororata Fault ruptures to further assess the likelihood that the WIL Storage Pond site had been adversely impacted by tectonic tilting, and to place constraints on the amounts of tilt the site could experience if the Hororata Fault were to rupture. Based on these analyses and modelling, Mr Van Dissen concluded that the WIL Storage Pond site was unlikely to have been adversely impacted by tectonic tilting, and that future rupture of the Hororata Faults was likely to produce tilts that were well below the 80 cm/km tolerable limit established by Dam Watch Engineering for the WIL Storage Pond.

Despite the above, there was dispute at the Seismic Experts – Expert Witness Conference (16 September 2015: point 8) regarding the amount of tilting. GNS contended that their modelling indicated that movement up to 30 cm/km was possible: whereas, Ms Campbell put forward the possibility of higher rates of tilting.

To further investigate, and constrain, the amounts of tilt and strain that could be expected at the WIL Storage Pond site resulting from rupture of the Hororata Fault, GNS has undertaken additional ground deformation modelling. Dr Ian Hamling (GNS Science) carried out further elastic dislocation modelling (similar to the modelling previously described in Mr Van Dissen's July 2015 evidence), but investigating additional ranges of rupture parameters and locations for scenario Hororata Fault ruptures. In addition, Dr Charles Williams (also of GNS Science) undertook finite element modelling which enabled the incorporation of geological layering (such as loose gravel overlying weak rock overlying strong rock) into the ground deformation modelling. The additional modelling and results are described below.

4.2 ADDITIONAL ELASTIC DISLOCATION MODELLING OF GROUND DEFORMATION

The dip of the Hororata Fault is poorly constrained. This has been noted in previous evidence presented by Dr McVerry, Ms Campbell, and Mr Van Dissen. In the ground deformation modelling previously undertaken by GNS, we assumed a dip of either 30° or 60° to the NW. In our additional modelling we use data specifically from the Canterbury earthquake sequence to provide insight as to what a more appropriate dip might be for rupture of the Hororata Fault. Beavan et al. (2012) and Elliott et al. (2012) both present geodetically derived solutions for the fault planes that ruptured in Canterbury earthquake sequence. Table 4.1 shows the dips, and top and bottom depths of rupture of the fault planes that had a reverse sense of displacement (like that which is anticipated for the Hororata Fault) or a significant component of reverse displacement. The average dip of the fault planes that ruptured in the Canterbury earthquake sequence that had a reverse sense of displacement (or a significant component of reverse displacement) is 65° with a standard deviation of about 10°. In our additional elastic dislocation ground deformation modelling, we evaluate three Hororata Fault dips: 55°, 65°, and 75° (all to the NW), with 65° being our preferred option. Essentially, we consider that the Canterbury earthquake sequence provides the strongest data available on which to judge what an appropriate dip might be for the poorly constrained Hororata Fault.

Table 4.1 also shows that the average top depth of rupture is ~1 km. In our additional elastic dislocation modelling, we entertain three top depths of rupture for scenario Hororata Fault ruptures: 0.5 km, 1.0 km, and 1.5 km. We also assume, like in our previous modelling, a bottom depth of rupture of 10 km.

We entertain two different Hororata Fault slip distributions: 1) uniform slip of 3 m (like in our previous modelling), and 2) variable slip averaging 3 m with approximately the bottom third of the fault plane having 5 m of slip, the middle third of the fault plane having 3 m of slip, and the top third of the fault plane having 1 m of slip. The variable slip scenario acknowledges the fact that slip during most large earthquakes is greater at depth than it is near the ground surface. In all our models, slip is assumed to be pure reverse dip-slip.

As discussed in Mr Van Dissen's July 2015 evidence, and agreed on at the Seismic Experts – Expert Witness Conference (16 September 2015: point 5), there is a gentle anticline mapped across the alluvial terrace/fan surface southeast of the WIL Storage Pond site (e.g., Forsyth et al. 2008, Barrell and Begg 2013) (Figure 4.1). (An anticline is a fold that is convex upwards.) The WIL Storage Pond site is ~3 km to the NW from the crest of this gentle anticline. In our additional modelling, we take the position of the crest of this anticline as marking the location of peak vertical ground surface deformation resulting from scenario Hororata Fault ruptures at depth.

Utilising the state-of-the-practice elastic dislocation formula of Okada (1985) and using a Poissons ratio of 0.25 and a shear modulus of 30 GPa, we calculate the ground surface displacements (including tilts and strains) at the WIL Storage Pond site for scenario reverse fault ruptures (with rupture parameters outlined in the previous paragraphs) that would generate maximum vertical deformation (i.e., generate an anticline crest) at the ground surface ~3 km SE from the WIL Storage Pond site.

An example of our elastic dislocation model set-up, and modelled results, are shown in Figure 4.2. Tables 4.2 lists the maximum gradients and horizontal and vertical strains across the WIL Storage Pond site resulting from the 9 additional scenario fault ruptures involving 3 m of uniform fault slip. Table 4.3 lists the maximum gradients and horizontal and vertical strains across the WIL Storage Pond site resulting from the 9 additional scenario fault ruptures involving variable fault slip. In all 18 cases, tilts at the WIL Storage Pond site range between 12–18 cm/km, and horizontal and vertical strains are small, ranging between 10^{-5} to 10^{-7}. (A strain of 10^{-5} is equivalent to centimetres of line-length change over a distance of one kilometre; a strain of 10^{-7} is equivalent to millimetres of line-length change over 10 km).

All the ground-surface deformation gradients listed in Tables 4.2 and 4.3 are well below the tolerable 80 cm/km limit, as provided to me by Mr Connell (Dam Watch Engineering). Mr Connell has also informed me that ground strains of 10^{-5} to 10^{-7} are able to be accommodated by the proposed dam embankments and linings.

It is relevant to note that the ground deformation modelling results presented in Figure 4.2 (and Tables 4.2 and 4.3) assume that the WIL Storage Pond site is located along the central portion of the Hororata Fault. This may, in fact, not be the case. It is possible that the WIL Storage Pond site is located at, or near, the northeastern termination of the fault [see geological map of Forsyth et al. (2008), Figures 2 and 9 of Dorn et al. (2010), and Figure 1 of Campbell et al. (2012)]. The gentle anticline southeast of the WIL Storage Pond site appears to die-out to the east-northeast and cannot be traced with any degree of confidence further to the east-northeast than depicted in Figure 4.1; whereas, to the southwest, on the opposite side of the Waimakariri River, the Racecourse Hill Anticline (the anticline that likely marks the surface expression of the Hororata Fault at depth) is a distinct and obvious topographic feature across terrace/fan surfaces of similar ages to those near the WIL Storage Pond site. Figure 4.2 shows that modelled ground deformations reduce rapidly near the terminations of rupture. If the WIL Storage Pond site is located at, or near, the northeastern termination of Hororata Fault rupture, then the tilts listed in Tables 4.2 and 4.3 may be overestimates.

4.3 FINITE ELEMENT MODELLING OF GROUND DEFORMATION

To examine the possible effects of material property variations and inelastic material behaviour on modelling ground deformations at the WIL Storage Pond site resulting from rupture of the Hororata Fault, we used the finite element code PyLith (Aagaard et al. 2013, 2015), which was specifically designed for the solution of tectonic problems. Of particular interest are the weak gravel layers in the near surface, which are unlikely to behave elastically, and the relatively low-strength (weak) sedimentary rocks underlying them. To model the potential effects of these weaker layers, we created two-dimensional plane strain quasi-static finite element models. The top two layers in our finite element models (Figure 4.3) represent gravel (a loose gravel layer over a dense gravel layer) and were characterised as Drucker-Prager elastoplastic materials. This rheology is commonly used to model brittle behaviour in the earth (e.g., Cattin et al. 2005), and indeed it was originally designed to represent the mechanics of soil (Drucker and Prager 1952). It is thus an appropriate rheology to model brittle/plastic behaviour of gravels. The third layer in our finite element model represents weak "Tertiary" rock. This layer, and the underlying strong Torlesse bedrock (layer 4) were modelled as elastic materials. The layer material properties used in the modelling are listed in Table 4.4. Note that PyLith directly uses P-wave velocity (Vp), shear-wave velocity (Vs), and density to compute elastic properties, so these are the values listed in Table 4.4. Layer thicknesses depicted in Figure 4.3, and listed in Table 4.4, are indicative averages derived from the cross-sections in Dorn et al. (2010) nearest to the site. We make no claim that these layer thicknesses characterise the exact conditions under the WIL Storage Pond site, but they more than adequately suffice to illustrate what impact the varying material properties and inelastic behaviours encompassed by the gravels and rocks that underlie the WIL Storage Pond site have on modelling ground deformation at the site.

We created two finite element meshes for this work. An example of one of these is shown in Figure 4.3. One mesh had a fault dipping at 65° NW, and the other included a fault with a dip of 55° NW. Material boundaries were placed at 100 m, 300 m, and 800 m depth. Fault slip was restricted to 10 km depth. To avoid effects due to boundary conditions, the mesh domain (70 km wide x 50 km deep) was made considerably larger than the region of interest. Roller boundary conditions were enforced on the vertical edges and bottom of the finite element mesh. Since the elastoplastic rheology is pressure-dependent, we also included gravitational body forces, using the densities from Table 4.4. For each fault dip, we tried six different coseismic slip distributions. Three of the slip distributions included constant reverse slip of 3 m, with top depths of rupture of 0.5 km, 1 km, and 1.5 km. The other three distributions had variable slip, with a slip of 5 m from 10 to 7 km depth, slip of 3 m from 7 to 4 km depth, and slip of 1 m from 4 km to the top depth of rupture. The fault dips, slip distributions, and top and bottom depths of rupture considered in our finite element modelling are comparable to those used in our elastic dislocation modelling described above in Section 4.2.

In addition to the layered models using elastoplastic rheology, we also performed simulations using homogeneous elastic materials, to evaluate the effects of the variable material properties. Note, when using the same fault rupture parameters, the ground deformation results derived from our finite element modelling using homogeneous elastic materials were nearly identical to the results derived from our elastic dislocation modelling.

Figure 4.4 shows an example of ground deformation results – vertical displacement, tilt, and horizontal strain – for the case of a 55° NW dipping scenario Hororata Fault rupture with 3 m of uniform (constant) slip. Figure 4.5 shows results for a 65° NW dipping Hororata Fault rupture with 3 m of constant slip. Figure 4.6 and Figure 4.7 show results for, respectively, a 55° NW dipping Hororata Fault rupture with variable slip, and a 65° NW dipping Hororata Fault rupture with variable slip. The important feature to note is the difference, or lack of difference, in ground surface deformation behaviour at the WIL Storage Pond site between the results derived from the layered (plastic) models (dashed lines in Figure 4.4–Figure 4.7), and those derived from the homogeneous (elastic) models (solid lines in Figure 4.4–Figure 4.7). As with our additional elastic dislocation modelling (Figure 4.3, Table 4.2 and Table 4.3), the WIL Storage Pond site is estimated to lie ~3 km northwest from the peak vertical ground displacement (i.e., anticline crest) resulting from rupture of the Hororata Fault at depth. In Figure 4.4–Figure 4.7 we observe that, although the layered (plastic) models predict some differences in displacements, tilts, and horizontal strain near the location where the fault would project to the ground surface (0 distance in Figure 4.4–Figure 4.7), the differences between the layered (plastic) and homogeneous (elastic) results become negligible at the location of the WIL Storage Pond site. For all of the models evaluated, we predict tilts of less than 20 cm/km at the WIL Storage Pond site, and horizontal strains of less than 50 µstrain (5.0×10^{-5} strain), comparable to the values listed in Table 4.2 and Table 4.3.

In our finite element modelling, we specifically chose material properties for the gravel layers (layers 1 and 2 in Table 4.4) that are conservative so as to accentuate the impact that these weak layers would have on the ground deformation results at the WIL Storage Pond site. In actuality, the gravel layers could have considerable higher densities, and higher Young's Moduli. Nevertheless, even using the conservative material properties for the gravel layers, the differences in the deformation results between the layered (plastic) models, and the homogeneous (elastic) models are negligible at the WIL Storage Pond site (Figure 4.4–Figure 4.7). If gravel layers were denser and "stiffer", the differences in the deformation results between the layered (plastic) models, and the homogeneous (elastic) models would be even more negligible at the WIL Pond site.

4.4 ADDITIONAL TOPOGRAPHIC ANALYSES

At the Seismic Experts – Expert Witness Conference (16 September 2015: point 8) it was agreed that:

"The amount of tilting and stretching is under dispute;

a. Modelling undertaken by GNS Science indicates movement of up to 30 cm/km

b. But, investigation by Ms Campbell suggests the possibility of a higher rate of tilting of up to 2 m/km. The change in gradient is not necessarily the consequence of a single event and includes some element of gradual change."

Ms Campbell's suggestion of the possibility of higher rates of tilting was based primarily on her interpretation of variations in fine-scale topography at and immediately east of the WIL Storage Pond site.

In order to investigate the credibility of the possibility of differential tilt of up to 2 m/km immediately east of the WIL Storage Pond site, we have constructed a Lidar-based topographic profile that extends for approximately 6 km in an east-southeast direction (i.e., down the depositional gradient), starting from the approximate western boundary of the WIL Storage Pond site. Figure 4.8 shows the location of this new profile (Profile X – X'), as well as the location of profiles previously presented in evidence by Mr Van Dissen. Figure 4.9 presents topographic Profile X – X' (blue line in Figure 4.9). Also shown in Figure 4.9 is the best-fit straight line (red line) through Profile X – X'. The best-fit line has a constant gradient of 7.6 m/km (sloping down to the east-southeast, and approximating the depositional gradient of the alluvial fan on which the WIL Storage Pond site is located). It is important to note that at no point does the ground surface along Profile X – X' deviate by more than 1 m above or below the best-fit line. It is difficult to imagine that the topography through the WIL Storage Pond site, and for an additional ~5 km to the east-southeast, would so closely follow a straight line if it had been subjected to folding and differential tectonic tilting of up to 2 km/m. The incredible straight-line fit of the topography depicted in Profile X – X' strongly suggests that the ground surface through the WIL Storage Pond site, and for several kilometres to the east-southeast, has been unaffected by folding and differential tectonic tilting. It is highly likely that the variations in fine-scale topography immediately east-southeast of the WIL Storage Pond site owe their origins to depositional and erosional processes driven by water and wind (as has previously been discussed in evidence presented by Mr Van Dissen), rather than to tectonic folding and differential tilting.

4.5 DISCUSSION AND CONCLUSIONS REGARDING GROUND-SURFACE FAULT RUPTURE HAZARD AT THE WIL STORAGE POND SITE

In light of the above, GNS concludes that within the resolution of the detailed DEMs and topographic profiles presented above (and previously as evidence by Mr Van Dissen) there is no direct evidence that surface fault rupture deformation expressed as either discrete faulting (i.e., a fault scarp) or km-scale wavelength folding (anticlinal or synclinal) has impacted the location of the WIL Storage Pond site within the last approximately 18,000 years.

There are three main alternative scenarios arising from the above conclusion:

1. the Hororata Fault, including possibly associated structures, does not extend beneath, or near to, the WIL Storage Pond site; or
2. the Hororata Fault, including possibly associated structures, does extend beneath, or near to, the WIL Storage Pond site but movement on the fault has not deformed the ground surface at WIL Storage Pond site within the last approximately 18,000 years; or
3. the Hororata Fault does extend beneath, or near to, the WIL Storage Pond site and movement on the fault at depth has deformed the ground surface at the WIL Storage Pond site within the last approximately 18,000 years, but these ground deformations have been of low gradient and low intensity. Modelling of co-seismic ground surface deformations (both tilts and strains) resulting from a wide range of scenario Hororata Fault ruptures indicate that the ground tilts and strains at the WIL Storage Pond site produced by those ruptures are likely to be well below the tolerable limits for the proposed dam embankments and liners.

Table 4.1 Fault dip and depth extents of geodetically determined fault plane solutions from the Canterbury earthquake sequence for faults that ruptured with a reverse sense of displacement or a significant component of reverse displacement.

Segment name	Dip (°)	Sense	top depth (km)	bottom depth (km)	Average Displacement (m)
Beavan et al. (2012)					
d	70	Reverse	0.5	10.8	1.22
e	50	Reverse	0.5	8	1.12
i	75	Reverse	0.5	7.2	0.71
j	70	Right-lateral/ Reverse	0.5	8	0.95
k	78	Right-lateral/ Reverse	1	8.8	0.36
m	69	Reverse/ Right-lateral	1	9.3	0.46
Elliott et al. (2012)					
4	76	Right-lateral/ Reverse	0	14.3	3.4
7	59	Reverse	1	8.5	4.5
8	46	Reverse	1.3	5.6	2.3
9	59	Reverse	3	6.7	3
average	65		0.9	8.7	1.8
stdev	11		0.8	2.3	1.3

Table 4.2 Tilt and strain at WIL Storage Pond site resulting from scenario ruptures of the Hororata Fault, based on elastic dislocation modelling and 3 m of uniform slip on the scenario fault planes.

Uniform slip							
Fault dip	**Top depth of rupture (km)**	**WIL Pond Site**				**Distance from crest of modelled anticline to projection of fault at ground surface (km)**	**Distance from projection of fault at ground surface to WIL Storage Pond site (km)**
		Tilt (cm/km)	**Strain**				
			ε_{Hperp}*	**ε_{Hpara}****	**ε_{V}*****		
55°	0.5	16.6	1.8×10^{-5}	4.0×10^{-6}	-7.5×10^{-6}	0.9	3.9
	1	17.3	-2.2×10^{-6}	4.2×10^{-6}	-6.6×10^{-7}	1.7	4.7
	1.5	17.6	-1.1×10^{-5}	4.2×10^{-6}	1.7×10^{-6}	2.3	5.3
65°	0.5	17.8	4.4×10^{-5}	3.6×10^{-6}	2.1×10^{-6}	0.9	3.9
	1	17.3	-2.9×10^{-5}	3.8×10^{-6}	8.6×10^{-6}	1.6	4.6
	1.5	16.6	-3.6×10^{-5}	3.8×10^{-6}	1.1×10^{-5}	2.1	5.1
75°	0.5	16.8	-3.5×10^{-5}	3.2×10^{-6}	1.1×10^{-5}	0.9	3.9
	1	15.7	-3.9×10^{-5}	3.4×10^{-6}	1.2×10^{-5}	1.5	4.5
	1.5	14.6	-3.8×10^{-5}	3.5×10^{-6}	1.2×10^{-5}	2	5
* ε_{Hperp} = Horizontal strain oriented perpendicular to fault strike							
** ε_{Hpara} = Horizontal strain oriented parallel to fault strike							
*** ε_{V} = Vertical strain							
Positive strain is extensional, and negative strain is contractional							

Table 4.3 Tilt and strain at WIL Storage Pond site resulting from scenario ruptures of the Hororata Fault, based on elastic dislocation modelling and variable slip on the scenario fault planes of 5 m of slip on approximately the bottom third of the fault plane, 3 m of slip on approximately the middle third of the fault plane, and 1 m of slip on approximately the upper third of the fault plane.

Variable slip							
Fault dip	Top depth of rupture (km)	WIL Pond Site				Distance from crest of modelled anticline to projection of fault at ground surface (km)	Distance from projection of fault at ground surface to WIL Storage Pond site (km)
		Tilt (cm/km)	Strain				
			ε_{Hperp}*	ε_{Hpara}**	ε_{V}***		
55°	0.5	16.4	2.6×10^{-6}	5.3×10^{-6}	-2.6×10^{-6}	4.7	7.7
	1	16.4	1.8×10^{-7}	5.3×10^{-6}	-1.8×10^{-7}	4.7	7.7
	1.5	16.5	-1.7×10^{-6}	5.4×10^{-6}	-1.2×10^{-6}	4.7	7.7
65°	0.5	14.1	2.7×10^{-6}	5.0×10^{-6}	-7.7×10^{-7}	3.9	6.9
	1	14.1	-6.9×10^{-6}	5.0×10^{-6}	6.4×10^{-7}	3.9	6.9
	1.5	14.1	-7.5×10^{-6}	5.0×10^{-6}	8.4×10^{-7}	3.9	6.9
75°	0.5	11.6	-1.2×10^{-5}	4.7×10^{-6}	2.5×10^{-6}	3.4	6.4
	1	11.6	-1.2×10^{-5}	4.7×10^{-6}	2.6×10^{-6}	3.4	6.4
	1.5	11.6	-1.2×10^{-5}	4.6×10^{-6}	2.3×10^{-6}	3.4	6.4
* ε_{Hperp} = Horizontal strain oriented perpendicular to fault strike							
** ε_{Hpara} = Horizontal strain oriented parallel to fault strike							
*** ε_{V} = Vertical strain							
Positive strain is extensional, and negative strain is contractional							

Table 4.4 Layer properties used in finite element modelling of ground surface deformation at the WIL Storage Pond site resulting from scenario ruptures of the Hororata Fault.

Material	Depths	Vp (m/s)	Vs (m/s)	Density (kg/m^3)	Cohesion (kPa)	Friction Angle	Poisson's ratio	Young's modulus	Reference
Layer 1: Loose gravel	0-100 m	313.4	127.9	1200	0	35°	0.40	55 MPa	1, 2
Layer 2: Dense gravel	100-300 m	376.3	180.8	1360	0	50°	0.35	120 MPa	1,2
Layer 3: Weak "Tertiary" rock	300-800 m	3574	2076	2370	N/A	N/A	N/A	N/A	3
Layer 4: Strong Torlesse bedrock	0.8-50 km	6512	3781	2924	N/A	N/A	N/A	N/A	4

References:
1, Bowles (1997); 2, Geotechdata.info, Angle of Friction; 3, Fry (unpublished 2013);
4, Eberhart-Phillips et al. (2010).

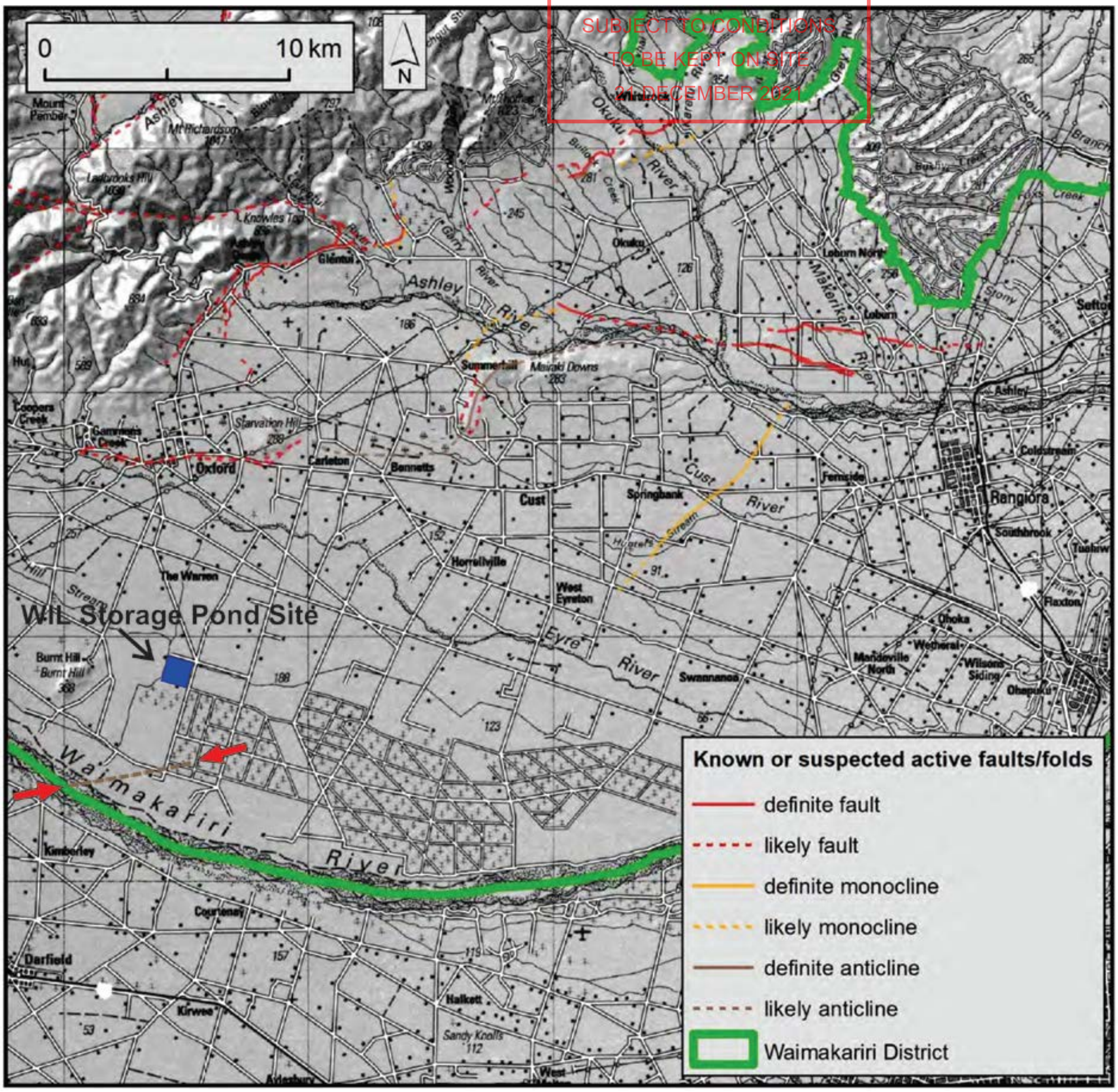

Figure 4.1 WIL Storage Pond site shown in relation tectonic features mapped by Barrell and Begg (2013). The red arrows denote the position of the gentle anticline referred to in main text that is located approximately 3 km southeast of the storage pond site.

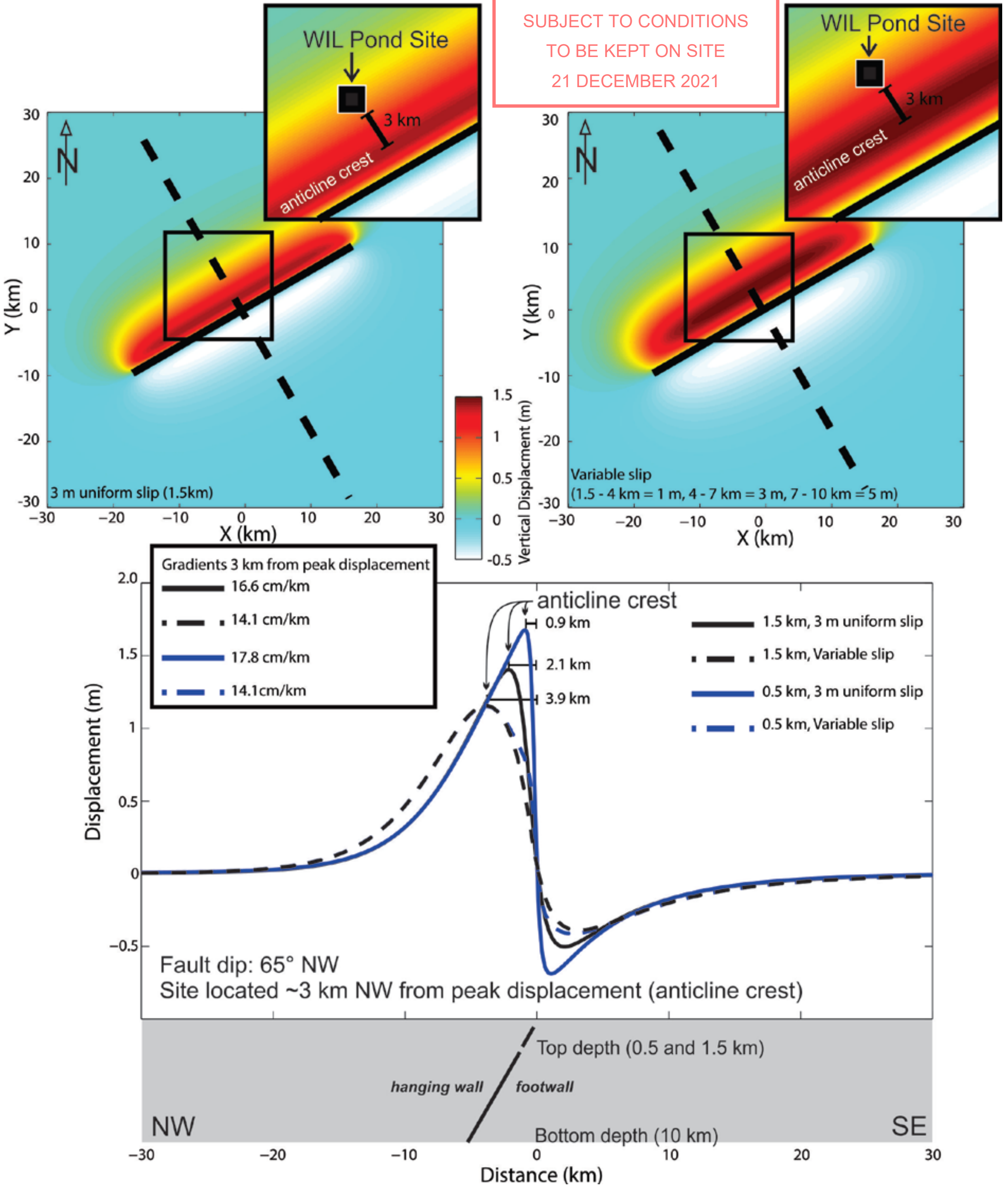

Figure 4.2 Surface displacements results for scenario Hororata Fault ruptures with uniform and variable reverse fault displacement. Top panels are map views with modelled vertical displacements at the ground surface colour coded according to the scale shown in the central part of the figure. Bottom panel shows profiles of vertical displacement at the ground surface oriented perpendicular to fault strike. The coloured key on the right indicates the scenario sources considered, while that on the left shows the resulting gradients for those scenarios at the WIL Storage Pond site. Resulting displacement gradients at the WIL Storage Pond site range between 14 cm/km to 18 cm/km for these four rupture scenarios. Note also the northwestward shift between the location of peak displacement (i.e., crest of anticline) and the up-dip projection at the ground surface of the buried fault at depth. For the models depicted in this figure, the shift ranges between 0.9 km to 3.9 km.

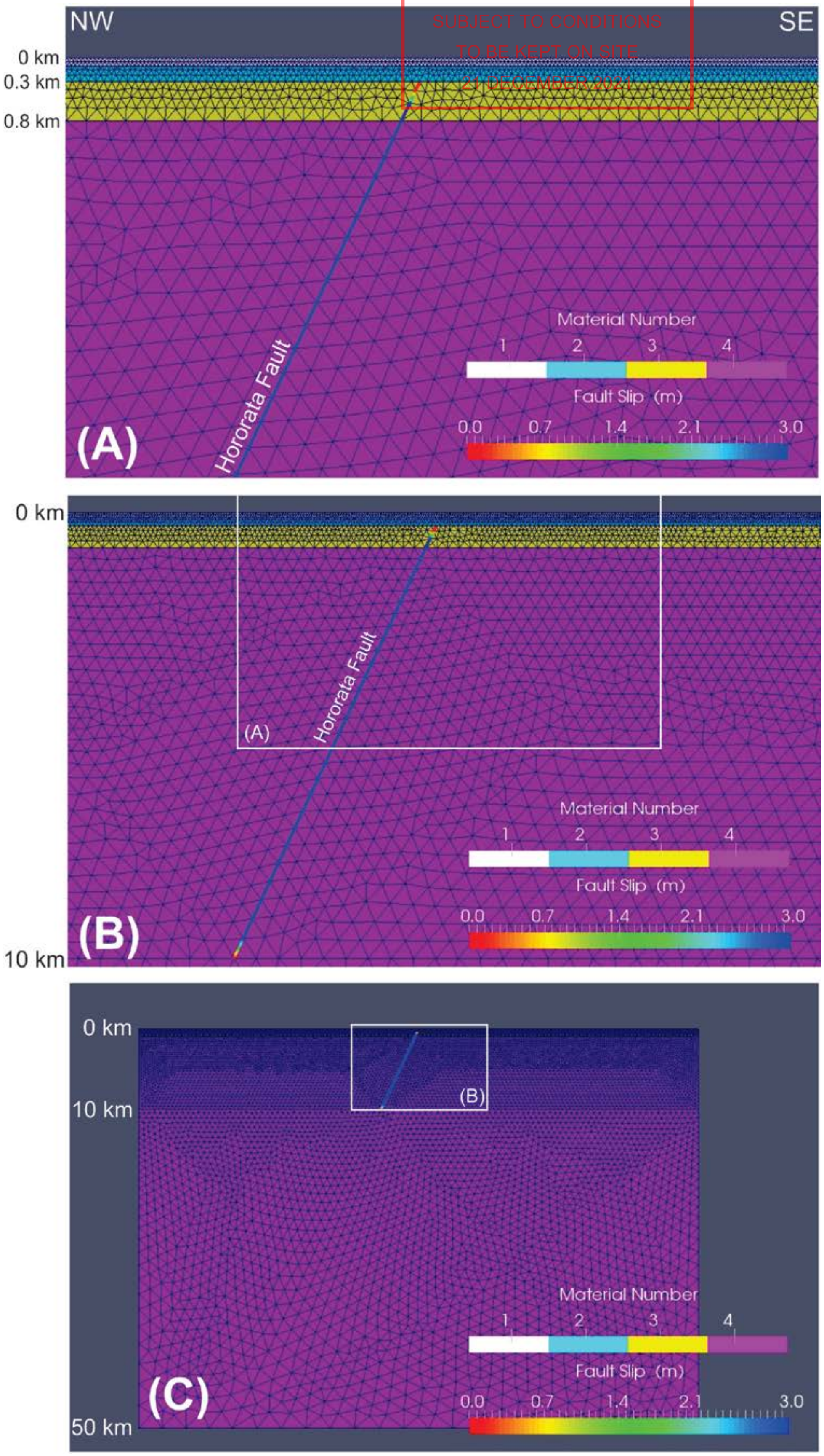

Figure 4.3 Example of finite element mesh used in ground deformation modelling. When the model is run using elastoplastic material properties, Layer 1 is parameterised as loose gravel, Layer 2 as dense gravel, Layer 3 as weak "Tertiary" rock, and Layer 4 as strong Torlesse bedrock. See Table 4.4 for listing of layer material properties.

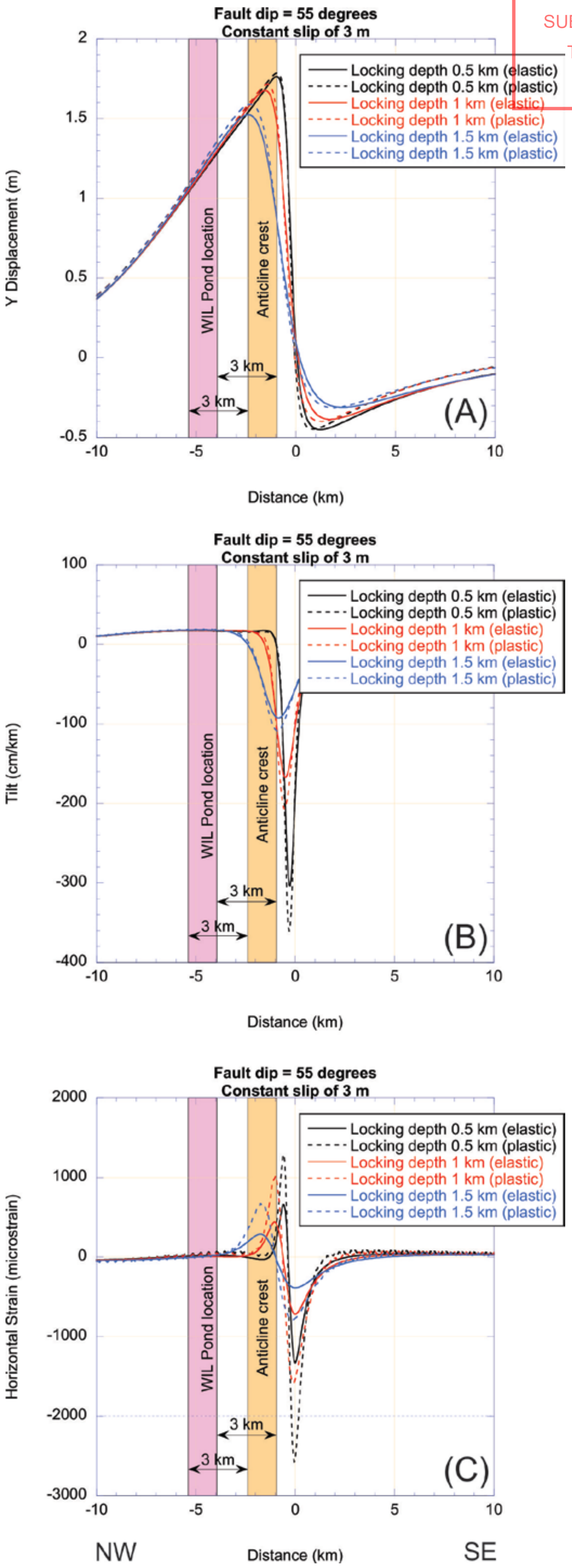

Figure 4.4 Finite element ground deformation results for the case of a 55° NW dipping scenario Hororata Fault rupture with 3 m of uniform (constant) slip. Dashed lines denote results derived from layered (plastic) models, and solid lines denote results derived from homogeneous (elastic) models. **A**) vertical displacement. **B**) tilt. **C**) horizontal strain.

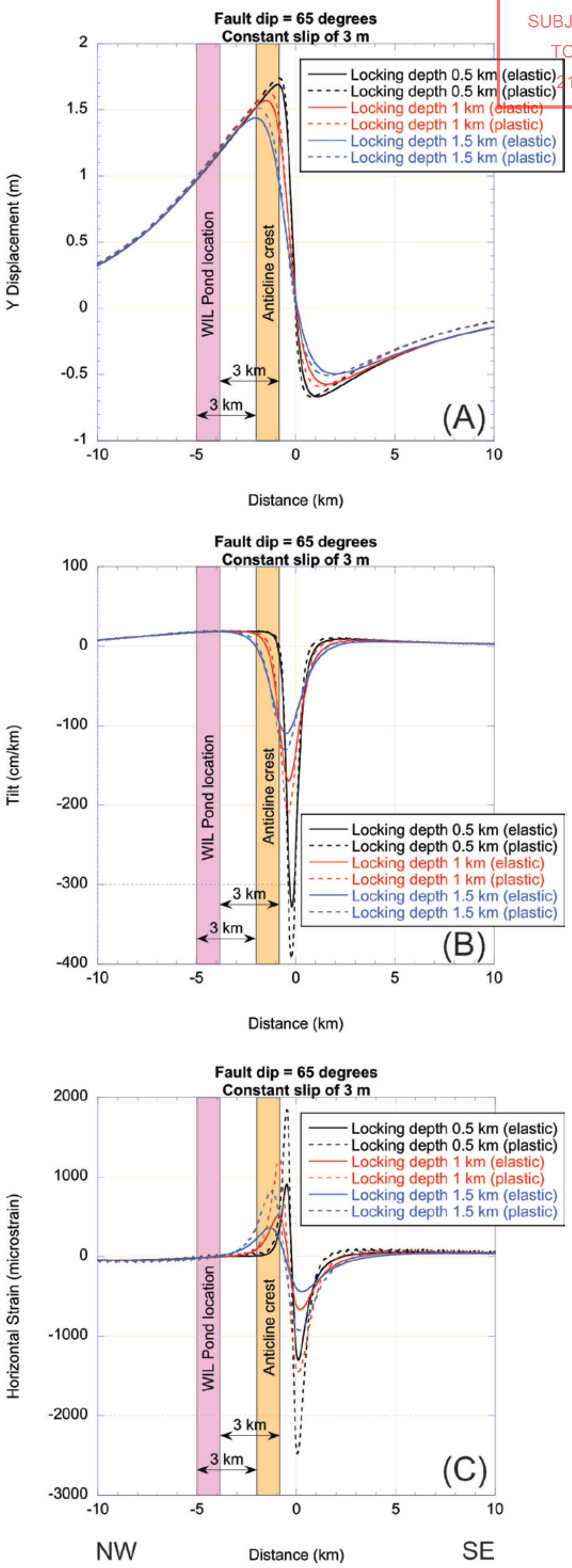

Figure 4.5 Finite element ground deformation results for the case of a 65° NW dipping scenario Hororata Fault rupture with 3 m of uniform (constant) slip. Dashed lines denote results derived from layered (plastic) models, and solid lines denote results derived from homogeneous (elastic) models. **A**) vertical displacement. **B**) tilt. **C**) horizontal strain.

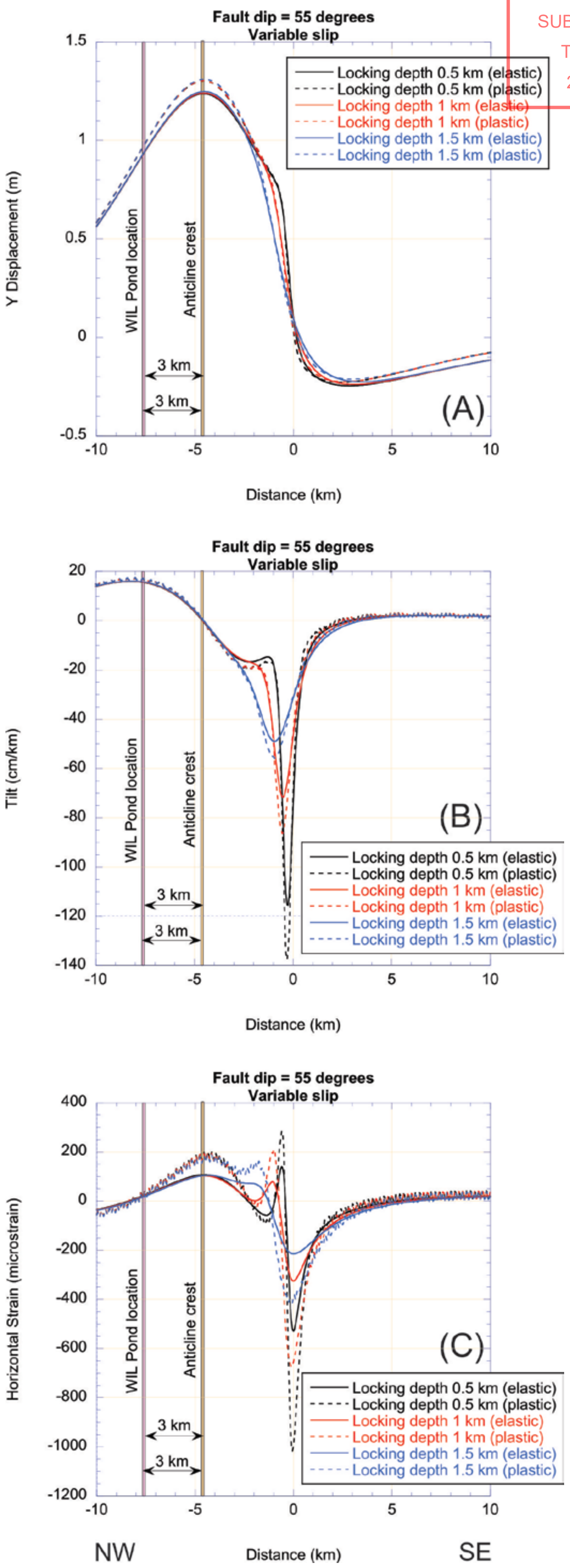

Figure 4.6 Finite element ground deformation results for the case of a 55° NW dipping scenario Hororata Fault rupture with variable slip (5 m of slip on approximately the bottom third of the fault plane, 3 m of slip on approximately the middle third of the fault plane, and 1 m of slip on approximately the upper third of the fault plane). Dashed lines denote results derived from layered (plastic) models, and solid lines denote results derived from homogeneous (elastic) models. **A**) vertical displacement. **B**) tilt. **C**) horizontal strain.

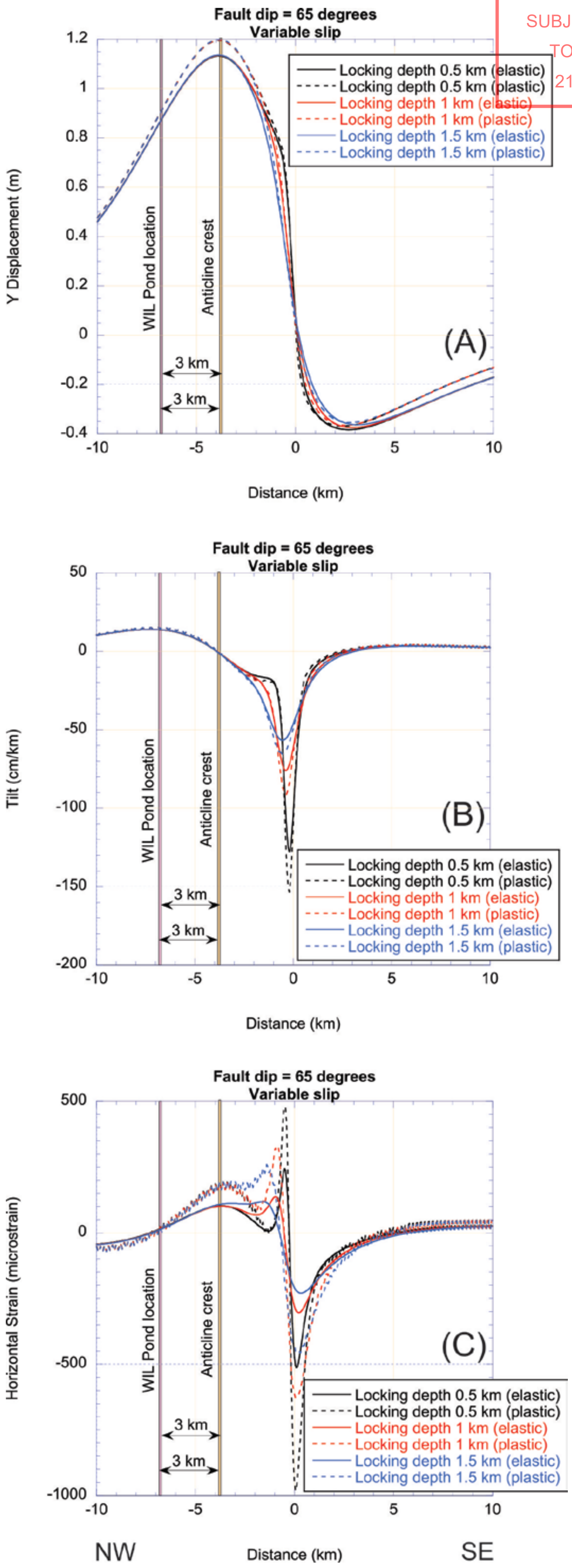

Figure 4.7 Finite element ground deformation results for the case of a 65° NW dipping scenario Hororata Fault rupture with variable slip (5 m of slip on approximately the bottom third of the fault plane, 3 m of slip on approximately the middle third of the fault plane, and 1 m of slip on approximately the upper third of the fault plane). Dashed lines denote results derived from layered (plastic) models, and solid lines denote results derived from homogeneous (elastic) models. **A**) vertical displacement. **B**) tilt. **C**) horizontal strain.

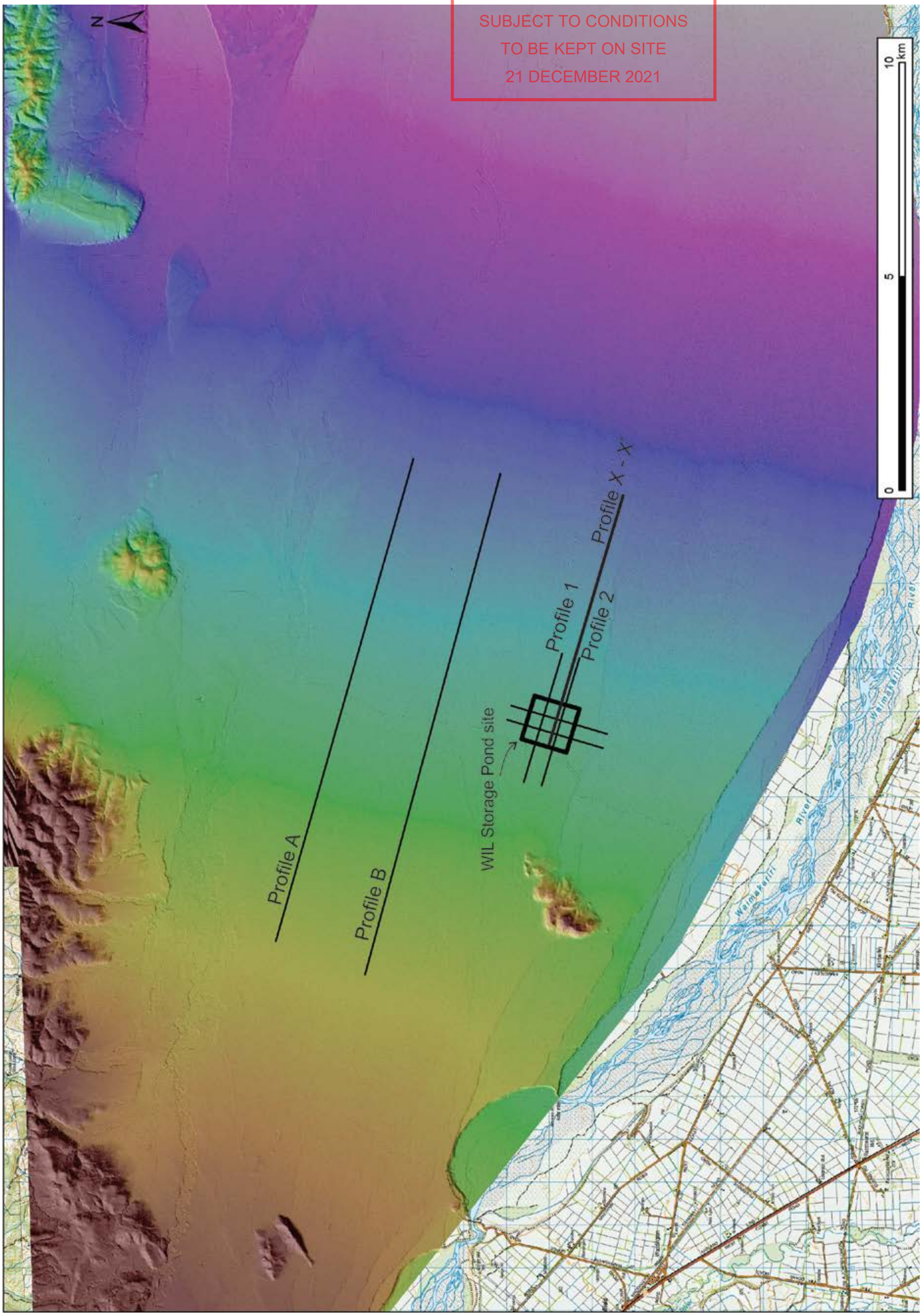

Figure 4.8 Location of topographic Profile X – X' through the WIL Storage Pond shown on the back-drop of a digital elevation model. Also shown are the locations of topographic profiles previously discussed in evidence presented by Mr Van Dissen.

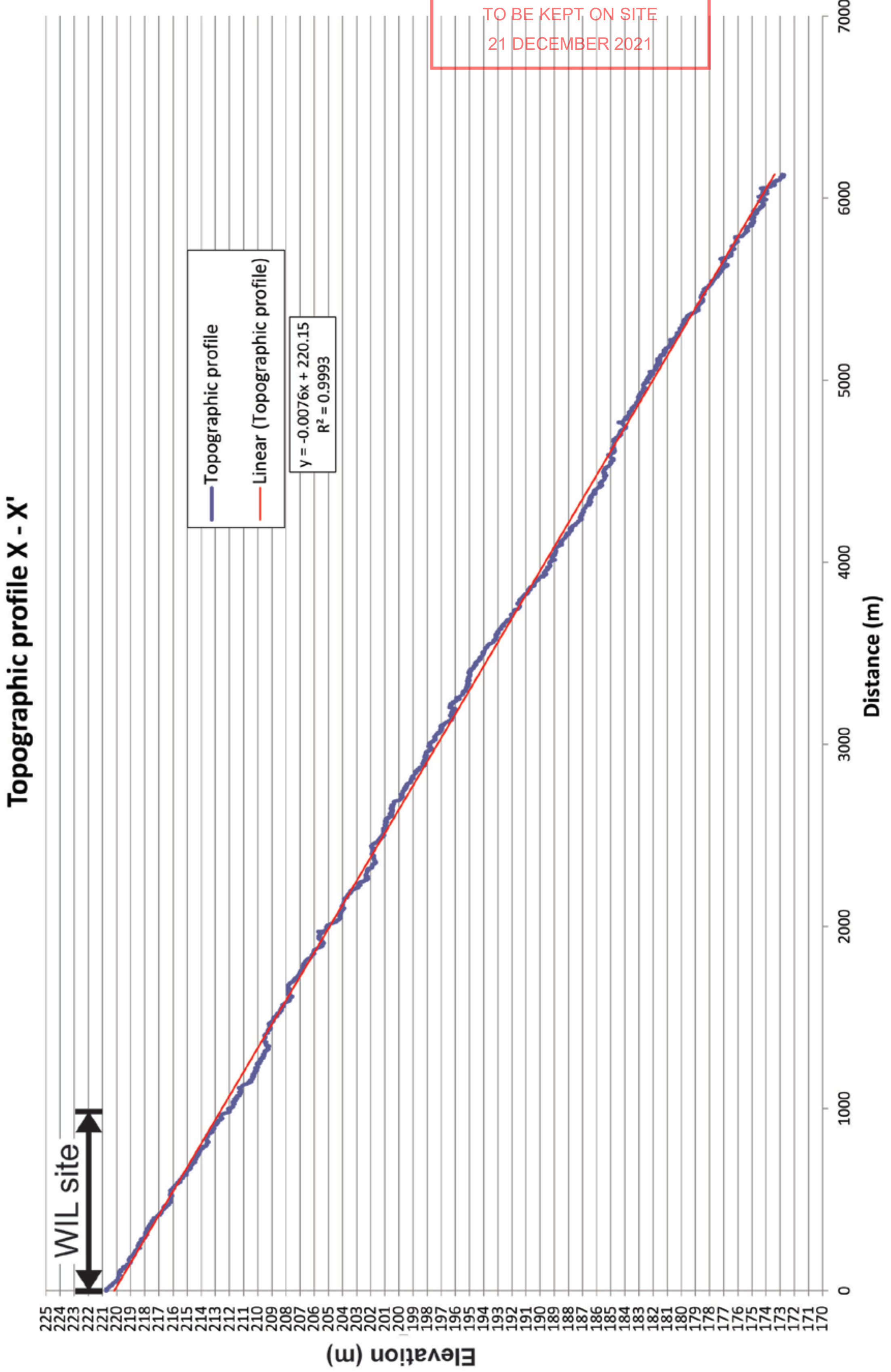

Figure 4.9 Topographic Profile X – X’ (blue line) based on Lidar data. Also shown is best-fit straight line (red line) through the topographic data.

5.0 CONCLUSIONS

The seismic hazard investigation undertaken in this report have reaffirmed and, importantly, substantiated conclusions previously presented as evidence by Dr McVerry and Mr Van Dissen, namely:

1. The design SEE pga of 1.11g based on the 1/10,000 AEP value derived from a probabilistic seismic hazard analysis is conservative and robust, and remains appropriate;
2. There is no direct evidence that surface fault rupture deformation expressed as either discrete faulting (i.e., a fault scarp), km-scale wavelength folding (anticlinal or synclinal), or differential tilting has impacted the location of the WIL Storage Pond site within the last approximately 18,000 years;
3. Should the Hororata Fault rupture within the lifespan of the WIL Storage Pond, it is likely that the ground tilts and strains resulting from that rupture will be well within the tolerable limits of the storage pond structure.

6.0 REFERENCES

Aagaard, B.; Kientz, S.; Knepley, M.; Strand, L.; Williams, C. 2015. PyLith User Manual, Version 2.1.0. Davis, California, USA. Computational Infrastructure of Geodynamics. URL: geodynamics.org/cig/software/pylith/pylith_manual-2.1.0.pdf

Aagaard, B.T.; Knepley, M.G.; Williams, C.A. 2013. A domain decomposition approach to implementing fault slip in finite-element models of quasi-static and dynamic crustal deformation. *Journal of Geophysical Research*: Solid Earth 118. doi: 10.1002/jgrb.50217.

Abrahamson, N.; Silva, W.; Kamai, R. 2014. Summary of the ASK14 Ground Motion Relation for Active Crustal Regions, *Earthquake Spectra*, *30(3)*: 1025-1055.

Barrell, D.J.A.; Begg, J.G. 2013. General distribution and characteristics of active faults and folds in the Waimakariri District, North Canterbury. GNS Science Consultancy Report 2012/326; Environment Canterbury Report No. R13/28. Accessible at the Environment Canterbury website < www.ecan.govt.nz >; search term < earthquake fault information >

Beavan, J.; Motagh, M.; Fielding, E.J.; Donnelly, N.; Collett, D. 2012. Fault slip models of the 2010–2011 Canterbury, New Zealand, earthquakes from geodetic data and observations of postseismic ground deformation. *New Zealand Journal of Geology and Geophysics, 55(3)*: 207-221. doi: 10.1080/00288306.2012.697472.

Bowles, J.E. 1997. “Foundation Analysis and Design, 5th Edition”, McGraw-Hill.

Bradley B.A. 2010. NZ-specific pseudo-spectral acceleration ground motion prediction equations based on foreign models *Report No.2010-03, Department of Civil and Natural Resources Engineering*, University of Canterbury: Christchurch, New Zealand. 324.

Bradley, B.A. 2013. A New Zealand-Specific Pseudospectral Acceleration Ground-Motion Prediction Equation for Active Shallow Crustal Earthquakes Based on Foreign Models, *Bulletin of the Seismological Society of America*, *103(3)*: 1801-1822, doi: 10.1785/0120120021.

Campbell, K.; Bozorgnia, Y. 2014. NGA-West2 Ground Motion Model for the Average Horizontal Components of PGA, PGV, and 5% Damped Linear Acceleration Response Spectra, *Earthquake Spectra*, *30(3)*: 1087-1115.

Campbell, J.; Pettinga, J.; Jongens, R. 2012. The tectonic and structural setting of the 4th September 2010 Darfield (Canterbury) Earthquake sequence, New Zealand. *New Zealand Journal of Geology and Geophysics, 55(3)*: 155–168.

Cattin, R.; Doubre, C.; de Chabalier, D.B.; King, G.; Vigny, C.; Avouac, J.P.; Ruegg, J.C. 2005. Numerical modelling of quaternary deformation and post-rifting displacement in the Asal–Ghoubbet rift (Djibouti, Africa). *Earth and Planitary Science Letters, 239*: 352–367.

Chiou, B.; Youngs, R. 2014. Update of the Chiou and Youngs NGA Model for the Average Horizontal Component of Peak Ground Motion and Response Spectra, *Earthquake Spectra*, *30(3*): 1117-1153.

Donahue, J.; Abrahamson, N. 2014. Simulation-Based Hanging Wall Effects, *Earthquake Spectra*, *30(3)*: 1269-1284.

Dorn, C.; Green, A.G.; Jongens, R.; Carpentier, S.; Kaiser, A.E.; Campbell, F.; Horstmeyer, H.; Campbell, J.; Finnemore, M.; Pettinga, J. 2010. High-resolution seismic images of potentially seismogenic structures beneath the northwest Canterbury Plains, New Zealand. *Journal of Geophysical Research, 115*(B11303). doi:10.1029/2010JB007459

Drucker, D.C.; Prager, W. 1952. Soil Mechanics and Plastic Analysis or Limit Design. *Quarterly of Applied Mathematics, 10(2):* 157-165.

Eberhart-Phillips, D.; Reyners, M.; Bannister, S.; Chadwick, M.; Ellis, S., 2010. Establishing a versatile 3-D seismic velocity model for New Zealand. *Seismological Research Letters, 81(6)*: 992–1000. doi:10.1785/gssrl.81.6.992.

Elliott, J.R.; Nissen, E.K.; England, P.C.; Jackson, J.A.; Lamb, S.; Li, Z.; Oehlers, M.; Parsons, B.; 2012. Slip in the 2010–2011 Canterbury earthquakes, New Zealand. *Journal of Geophysical Research*: Solid Earth, *117(B03401)*. doi: 10.1029/2011JB008868.

Forsyth, P.J.; Barrell, D.J.A.; Jongens, R. (comps) 2008. Geology of the Christchurch area: scale 1:250,000. Lower Hutt: GNS Science. Institute of Geological & Nuclear Sciences 1:250,000 geological map 16. 67 p. + 1 folded map.

Fry, B. 2013. Unpublished one-dimensional seismic velocity model for Canterbury region. GNS Science.

Geotechdata.info, Angle of Friction, http://geotechdata.info/parameter/angle-of-friction.html (as of September 14, December, 2013).

Gerstenberger, M.C.; McVerry, G.; Rhoades, D.A.; Stirling, M. 2014, Seismic Hazard Modelling for the Recovery of Christchurch, New Zealand. *Earthquake Spectra, 30(1)*: 17-29. (Canterbury Special volume)

Hornblow, S.; Quigley, M.; Nicol, A.; Van Dissen, R.; Wang, N. 2014. Paleoseismology of the 2010 Mw 7.1 Darfield (Canterbury) earthquake source, Greendale Fault, New Zealand. *Tectonophysics 637:* 178-190. http://dx.doi.org/10.1016/j.tecto.2014.10.004.

McVerry, G.H; Zhao, J.X.; Abrahamson, N.A.; Somerville, P.G. 2006. New Zealand acceleration response spectrum attenuation relations for crustal and subduction zone earthquakes. *Bulletin of the New Zealand Society for Earthquake Engineering*; *39(4):* 1-5.

NZSOLD 2015. *New Zealand Dam Safety Guidelines*. New Zealand Society on Large Dams, Wellington, New Zealand. ISBN: 978-0-908960-65-1.

Okada, Y. 1985. Surface deformation due to shear and tensile faults in a half-space. *Bulletin of the Seismological Society of America, 75(4)*: 1135-1154.

Stirling, M.W.; McVerry, G.H.; Gerstenberger, M.C.; Litchfield, N.J., Van Dissen, R.J.; Berryman, K.R.; Barnes, P.; Wallace, L.M.; Villamor, P.; Langridge, R.M.; Lamarche, G.; Nodder, S.; Reyners, M.E.; Bradley, B.; Rhoades, D.A.; Smith, W.D.; Nicol, A.; Pettinga, J.; Clark, K.J.; Jacobs, K. 2012. National seismic hazard model for New Zealand: 2010 update. *Bulletin of the Seismological Society of America*, *102(4):* 1514-1542; doi: 10.1785/0120110170.

GNS SCIENCE
TE PŪ AO

www.gns.cri.nz

Principal Location

1 Fairway Drive
Avalon
PO Box 30368
Lower Hutt
New Zealand
T +64-4-570 1444
F +64-4-570 4600

Other Locations

Dunedin Research Centre
764 Cumberland Street
Private Bag 1930
Dunedin
New Zealand
T +64-3-477 4050
F +64-3-477 5232

Wairakei Research Centre
114 Karetoto Road
Wairakei
Private Bag 2000, Taupo
New Zealand
T +64-7-374 8211
F +64-7-374 8199

National Isotope Centre
30 Gracefield Road
PO Box 31312
Lower Hutt
New Zealand
T +64-4-570 1444
F +64-4-570 4657